Terahertz Vibrational Modes of Inverse Micelles

Joel E. Boyd,[†] Ari Briskman,[‡] Christie M. Sayes,[†] Daniel Mittleman,*[,‡] and Vicki Colvin[†]

Department of Chemistry, and Department of Electrical and Computer Engineering, Rice University, Houston, Texas 77251

Received: January 29, 2002; In Final Form: April 5, 2002

A large absorption resonance has been observed in the far-infrared spectrum of water confined within inverse micelles of sodium bis(2-ethylhexyl) sulfosuccinate (AOT) in heptane. The amplitude and spectral position of this resonance depend on the size of the water pool. The origin of the THz absorption of these liquid pools is assigned to surface oscillations of the water pool, driven by the interfacial tension of the water−surfactant-oil interface. These data indicate a dramatic restructuring of the density of states of the liquid and are consistent with a theoretical model for the oscillatory modes of liquid droplets. The presence of a large excess in the vibrational density of states of confined water could have far-ranging implications in many biochemical and chemical processes where confined water is present.

Introduction

The properties of water confined on the nanometer scale are important in a diverse range of disciplines. Many processes in biology and chemistry occur within water cavities of nanometer-sized dimensions. Biological macromolecules, most notably proteins, not only function in aqueous environments but also contain large fractions of water within their structure. This "bound" water can consist of only a few water molecules or more than several hundred. Its presence is crucial for many functions of biological systems;[1−10] yet, the most basic properties, such as density and dielectric constant, cannot readily be characterized in-situ. Confined water is also frequently encountered in areas of materials processing. Many high surface area catalysts possess small cavities where chemical reactions are accelerated;[11−13] quantitative predictions for reaction rates in these systems require some estimate of the solvent's properties. Also, nanoscale reactors defined by inverse micelles have become a popular route to the formation of nanocrystalline materials.[14−17] As it becomes more important to affect quantitative control over reaction rates in these media, many fundamental properties of water in these environments will need to be characterized.

An excellent model system for confined water can be found in the water contained within inverse micelles. These are nanometer-sized water droplets stabilized in an oil phase by a surfactant.[6,18,19] We focus here specifically on micelles formed using the surfactant sodium bis(2-ethylhexyl) sulfosuccinate (AOT); this system has emerged as a model for inverse micelles. Extensive experimental and theoretical studies have developed a consistent picture of the local structure within these micelles. These systems provide three-dimensional confinement of water with well-controlled size distributions and evident biological relevance. AOT micelles can be formed with water pools ranging from essentially zero size to as many as 100 000 water molecules and have been extensively characterized so that size dispersion, interfacial organization, and interior water structure are well established.[20,18,21−24] One drawback to using inverse micelles for investigations of far-infrared dynamics is that they do not lend themselves well to temperature-dependent studies because the micelle size and stability are dependent upon temperature.[18] The wide range and controllability of their sizes, however, make them extremely attractive for studying confined water.

Infrared spectroscopy has been one of the most informative techniques applied to the study of water in these micelles. In particular, the OH-stretch region of the spectrum, near 3500 cm^{-1}, is sensitive to the structure of the hydrogen bond network and has been monitored as a function of micelle size.[25−29] The systematic changes in peak position and shape have been used to propose a model for the local structure of water in these micelles. This local microstructure has also been studied using a variety of NMR techniques.[21,30,31] Although providing a valuable description of the structure of the water core, these measurements give little information about the dynamical processes that may involve many water molecules. Instantaneous normal mode calculations confirm that the modes interrogated by these spectroscopic methods are not collective in nature[32] and are therefore not likely to be strongly perturbed by geometrical confinement.

A more sensitive probe of the effects of confinement can be found by studying collective modes, whose correlation length is comparable to or larger than the confinement length scale. This has recently been demonstrated in a study of the H_2O librational band, at ∼670 cm^{-1}; the spectral location of this band is extremely sensitive to the structural geometry of the hydrogen bond network.[33] Even more dramatic effects should be expected in the far-infrared below 100 cm^{-1}. The dielectric function of bulk water exhibits its primary relaxation features in the far-infrared region, between 1 and 100 cm^{-1}. The modes associated with these relaxation features are generally described in terms of a double Debye model[34] but are nevertheless thought to be highly collective in nature. Thus, far-infrared (terahertz) spectroscopy is an ideal tool for studying the effects of confinement on the mode spectrum of liquids.

Terahertz time-domain spectroscopy (THz-TDS) is a relatively new technique that permits the measurement of both the real and imaginary parts of the dielectric function over much

* To whom correspondence should be addressed. Phone: (713) 348-5452. Fax: (713) 348-5686. E-mail: daniel@rice.edu.
[†] Department of Chemistry.
[‡] Department of Electrical and Computer Engineering.

10.1021/jp0255740 CCC: $22.00
Published on Web 05/10/2002

of the far-infrared range. Other methods for accessing the low frequency modes of liquids include inelastic neutron scattering and Raman spectroscopy, which have been extensively used to characterize confined liquids.[24,35−37] However, neither of these techniques make a direct connection to the dielectric properties of the liquid. Far-infrared spectroscopy is a complementary technique that is well suited for probing the heterogeneous and complex geometries of three-dimensionally confined water. We have recently reported the observation that smaller AOT inverse micelles exhibit a dramatic restructuring of the mode spectrum.[38] Here we describe a more complete study of the far-infrared dielectric behavior of confined water along with discussion of its relevance and implications.

Experimental Section

Materials. AOT (99%) was purchased from Sigma and purified before use. Anhydrous heptane (Aldrich, 99%), dodecane (Aldrich, 99%), hexane (Aldrich, 95%), pentanol (Aldrich, 99%), glycerol (Aldrich, 99.5+ %), D_2O (Aldrich, 99.9%), and NaCl (Fisher) were all used as received. CTAB (Aldrich) was used in its commercially available form. Brij-30 (Fluka) is delivered cloudy and somewhat separated into two phases. It must be heated to 50 °C to homogenize the liquid surfactant before use.

AOT was purified before use based on the method of Martin and Magid.[39,40] Purified AOT was kept over P_2O_5 (Aldrich) in a vacuum desiccator at least 48 h before use. Karl Fisher titrations (Metrohm 701 KF Titrino) revealed that the residual water content before this purification process was 0.59 mol of water per mol of AOT, whereas after purification this dropped to less than 0.2 mol of water per mol of AOT. This process also removes organic compounds (e.g., alcohols), which can act as cosurfactants and lead to greater inhomogeneity. We have found that this purification process is crucial to obtain repeatable results in the experiments described below.

AOT samples were prepared by dissolution of known weights of AOT in 30−50 mL of heptane. Water (Millipore, 18.2 MΩ/cm^2) was then injected into the solution to make samples of varying w, where w is the concentration ratio $[H_2O]/[AOT]$. The samples were prepared so that the volume fraction of micelles in solution was 6%. For each hydrated sample, a reference sample, containing no added water, was formulated to contain an identical volume fraction of surfactant in solution.

Samples were used after stirring overnight and within 4 days of preparation to minimize hydrolysis of the surfactant. This is reported to occur upon prolonged surfactant−water contact.[41−43] Samples were formulated in 125 mL amber bottles with septa caps (Fisher) and were thoroughly stirred during formulation as well as immediately prior to any experimental measurement. The inverse micellar solutions were filtered through 0.2 micron pore-size Teflon syringe filters (Aldrich) while being dispensed for spectroscopic analysis. CTAB solutions were made in a manner similar to the AOT formulations; however, the solvent for these samples was a 60.6:8.65 molar ratio of hexane:pentanol.[44] The solvent for the Brij-30 experiments was dodecane. After stirring during formulation, the samples were clear, homogeneous solutions without any haziness and remained so for months after formulation in the case of the AOT samples. The exceptions to this sample clarity were CTAB and Brij-30 reference samples without water added to the solution. CTAB is insoluble in its solvent without the addition of water, and thus a small quantity of water (amounting to $w = 4$) was added to solubilize the surfactant. These samples were then completely clear after formulation. Brij-30 samples that were formulated without water were somewhat cloudy, although the surfactant did appear to be completely dissolved and showed no tendency to settle out of solution.

Methods

The far-infrared dielectric spectroscopic data were collected with a relatively new method, terahertz time-domain spectroscopy (TDS).[34,45,46] This method provides both the absorption and refractive index of a sample without resorting to a Kramers−Kronig analysis. The far-infrared (THz) radiation is coherently emitted and detected using femtosecond (fs) pulses from a 80 MHz titanium sapphire laser operating at 789 nm. These ultrashort pulses are focused onto antennae that consist of a pair of gold leads photolithographically deposited onto semiconductor (low-temperature-grown GaAs) substrates. The transmitter antenna is biased at 20 V; the acceleration of the electrons excited above the band gap by the fs pulse results in the emission of broadband radiation, with a spectrum covering the range from ∼0.1 to 1.5 THz. The THz pulse is then collimated by a combination of a hyperhemispherical silicon lens mounted directly onto the substrate and a high-density polyethylene lens. After passing through the sample, the THz beam is refocused onto the receiving antenna, which is not biased. The charge carriers created by the fs optical excitation within the receiver antenna gap are accelerated by the incoming THz field. The current measured across the receiving antenna is thus proportional to the amplitude of the THz electric field. The relative delay between the THz pulse and the optical pulse on the receiver can be varied to measure the waveform as a function of time via photoconductive sampling.[47,48] The current detected at the receiver is amplified by a current-to-voltage amplifier and then recorded using a lock-in amplifier which is queried by a computer via GPIB interface.

The sample is contained in a polyethylene bag which is inserted into a variable path length cell comprised of two high-density polyethylene windows; one of these windows is fixed, and the other is attached to a computer-controlled stepper motor. A complete scan is collected at each of a series of seven path lengths varying from 5 to 1 mm in thickness. The multiple path length data is then used to calculate both the refractive index (n) and absorption (α) of the sample, using the procedure outlined by Kindt and Schmuttenmaer.[34] The spectral range over which these quantities can be determined depends on the bandwidth of the radiation source and the absorption of the sample. Data points at frequencies where the amplitude of the signal is not at least 20 times greater than that of the noise spectrum are excluded from the analysis.

Results

Using terahertz time-domain spectroscopy, it is straightforward to measure the real and imaginary dielectric response of the micellar solutions as described above. These frequency-dependent dielectric values are related to the refractive index and absorption coefficient through the standard relations:

$$\epsilon'(\nu) = n(\nu)^2 - \kappa(\nu)^2 \quad (1)$$

$$\epsilon''(\nu) = 2n(\nu)\,\kappa(\nu) \quad (2)$$

where $\epsilon = \epsilon' - i\epsilon''$.[34]

Representative spectra are shown in Figure 1 for several micelle samples, with w values shown. Also shown for comparison are the same data for a nonhydrated reference

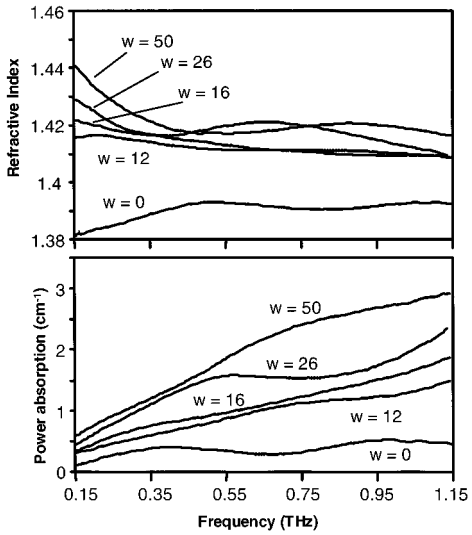

Figure 1. Refractive indices (upper panel) and power absorption coefficients (lower panel) for several representative micelle samples, with the *w* values shown, obtained using the terahertz time-domain spectroscopy technique described in the text. The $w = 0$ data sets show the results for a reference sample containing surfactant but with no water added.

sample (labeled $w = 0$). The presence of water in the hydrated samples leads to an increase in the overall sample absorption across the entire spectral range. This is not surprising because water has an absorption coefficient hundreds of times larger than heptane.[49,50]

The data shown in Figure 1 represent the dielectric response of the entire three-component solution. To extract the response of the water inside the inverse micelles, we must account for the dielectric effects of the solvent and surfactant shell and the spherical geometry. At these frequencies, this is more complicated than a simple background subtraction, because of the temporal response of the interfacial polarization at the spherical surface of the micelle.

To access the dielectric response of the water alone, a deconvolution is performed according to a core−shell dielectric model developed by Hanai et al.[51] This model is routinely employed in dielectric spectroscopy of colloidal and micellar solutions at gigahertz frequencies.[51−55] It is essentially equivalent to the well-known Lorentz electrostatic local field correction,[56] except that in our case there are three dielectric components rather than two. Here we apply it without alteration to the terahertz dielectric response of the water core. The model rests on several key assumptions. First, the inverse micelle is assumed to possess a spherical water core surrounded by a spherical shell of surfactant of uniform thickness. An additional assumption is that the dielectric spectrum of the surfactant shell is the same in hydrated and nonhydrated samples. This is a reasonable approximation because the geometry of the surfactant molecules is not strongly altered by hydration and the nonhydrated samples are known to form spherical micellar structures.[18,24] A more serious assumption involves the abruptness of the interfaces between the nonpolar phase and the surfactant and between the surfactant layer and the aqueous core of the micelle. The internal interface has been studied by molecular dynamics simulation, from which it is clear that it is only a few monolayers thick.[57] The external interface, involving the long hydrophobic tails of the AOT, is less well characterized. Despite this uncertainty, the core−shell model discussed here is a reasonable first approach to the problem of deconvolving the dielectric response.

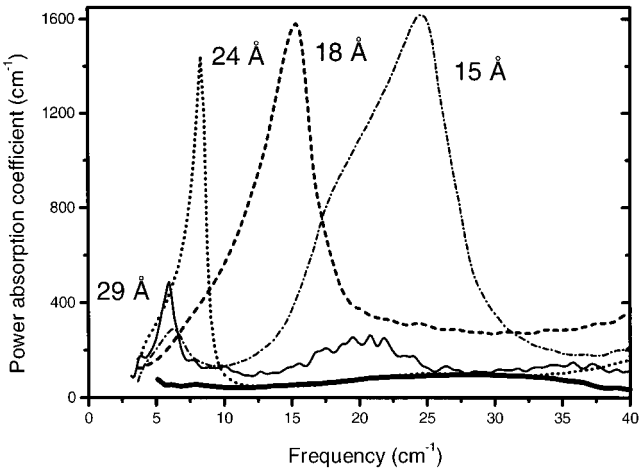

Figure 2. Absorption spectra of the aqueous core of several micelle samples, derived using the deconvolution procedure of eqs 3 and 4, as described in the text. The thick, nearly featureless curve at the bottom represents a radius of 75 Å, one of the largest micelles studied to date. All other curves correspond to the water pool radii as labeled.

If the dielectric of the background solvent is known, then the dielectric of the micelle is determined from

$$\frac{\epsilon_{\text{solution}} - \epsilon_{\text{micelle}}}{\epsilon_{\text{background}} - \epsilon_{\text{micelle}}}\left(\frac{\epsilon_{\text{background}}}{\epsilon_{\text{solution}}}\right)^{1/3} = 1 - \varphi \qquad (3)$$

where ϕ is the volume fraction of micelles in solution. From $\epsilon_{\text{micelle}}$, one can determine the dielectric of the core if the dielectric of the surfactant shell is known, using

$$\epsilon_{\text{micelle}} = \epsilon_{\text{shell}} \cdot \frac{2(1-\nu)\epsilon_{\text{shell}} + (1+2\nu)\epsilon_{\text{core}}}{(2+\nu)\epsilon_{\text{shell}} + (1-\nu)\epsilon_{\text{core}}} \qquad (4)$$

Here, ν is the volume fraction of the water core within the micelle, which is determined using literature values for the thickness of the AOT shell[21] and the water pool radius.[18] The dielectric of the shell is determined experimentally, by measuring the dielectric of a reference solution containing AOT but no water. As mentioned above, it is known that, even in the absence of water, the surfactant still forms spherical aggregates with the polar headgroups at the center.[18] With this knowledge of ϵ_{shell}, we can compute ϵ_{core}, the dielectric of the water in the interior of the micelle, from the measured spectra. ϵ_{core} can then be used to derive the absorption and refractive index of the encapsulated water using eqs 1 and 2.

In striking contrast to the relatively featureless dielectric spectrum of bulk water, the results of measurements of the inverse micellar water shows an extraordinarily large resonant absorption in the far-infrared. Figure 2 shows several of these absorption peaks at various micellar sizes. For a resonant absorption, a Cole−Cole plot of the real component of the dielectric function versus the imaginary component generates a circle. Figure 3 shows Cole−Cole plots for two representative data sets; the dashed curves are least-squares fits to circles, demonstrating the resonant nature of these excitations.

This absorption feature is only observed for micelles with radii between 15 and 45 Å. The spectra of larger micelles do not exhibit a discernible absorption peak but instead resemble the featureless absorption spectrum of bulk water. Both the amplitude and spectral position of the absorption peak depend on the size of the micelle. As the micelle size is increased, the peak frequency of the absorption moves from high frequency (∼1 THz at $R = 15$ Å) to lower frequencies (∼0.2 THz at $R =$

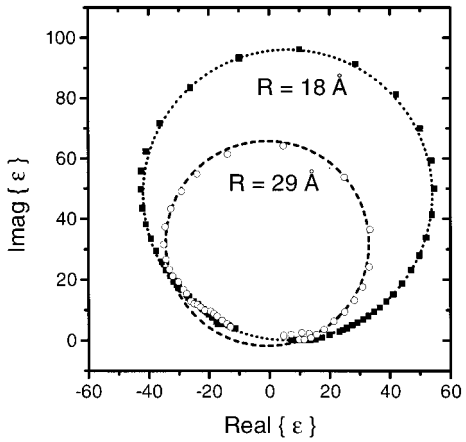

Figure 3. Cole−Cole plots of the imaginary part of the dielectric versus the real part, for two of the samples shown in Figure 2. The dashed curves are nonlinear least-squares fits of these data to circles. A circular Cole−Cole plot is indicative of a resonance.

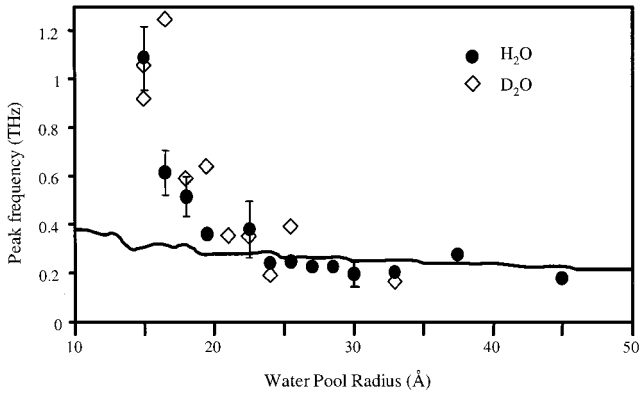

Figure 4. Spectral location of the absorption peak, as a function of water pool radius, for micelles made with both H_2O (solid circles) and D_2O (open diamonds). The solid curve is the mean value of the frequency of the surface-localized vibrational band, computed using the model described in the text. This a priori calculation contains no adjustable parameters.

45 Å). In addition, the amplitude of the peak decreases significantly as the micelle size is increased. Figure 4 shows the spectral position of the peak as a function of the radius of the internal water pool, whereas Figure 5 shows the measured absorption coefficient, integrated from 0.1 to 1.3 THz. This allows comparison of the absorption of these solutions with that of bulk water integrated over the same range, depicted by the dashed horizontal line. In addition to the striking size dependence shown in these two figures, it is interesting to note that the integrated absorption strength is *smaller* than that of bulk water for larger micelles.

AOT inverse micelles can also be formulated with polar liquids other than H_2O. The closest homologue available is obviously D_2O. Inverse micelles were formulated and measured containing D_2O instead of the usual H_2O. The far-infrared absorption spectra of these samples showed virtually no difference from the water micelles. Figure 4 is a comparison of the resonant frequency of the absorption peak of the D_2O inverse micelles compared with the H_2O inverse micelles.

Other nonaqueous polar liquids can be solubilized within the core of inverse micelles. Glycerol, a moderately strong glass-forming liquid, is readily incorporated into AOT microemulsions. Furthermore, this system has also been well characterized with respect to the concentration dependence of the micellar size. For glycerol in AOT, the appropriate relationship is R (Å) $= 8.8w$.[41] The stability range of glycerol-containing inverse micelles is limited to $w < 4$. This makes a thorough size-dependent study quite difficult, but nevertheless, it is possible to perform similar measurements to see if a resonance is present. Data are shown in Figure 6 for three glycerol samples, in which a pronounced peak is observed, similar to that observed in smaller aqueous micelles. The observation of absorption peaks in glycerol is very significant, as it demonstrates that the phenomenon is not limited to one specific chemical system.

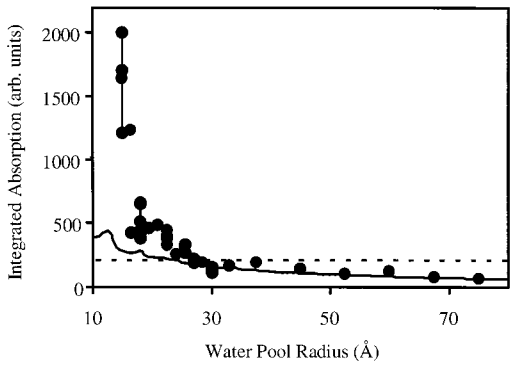

Figure 5. Data points represent the integrated absorption strength of the resonance peaks (such as those shown in Figure 2), as a function of water pool radius. These curves have been integrated over the range from 0.1 to 1.3 THz. The horizontal dashed line shows the value obtained from a similar integration of the spectrum of bulk liquid water. The solid curve represents the fraction of the total vibrational spectrum contained in the surface vibrations, computed using the surface modes model described in the text. This a priori calculation has been scaled by an overall multiplicative factor to match the value of the right-most data point (the 75 Å water pool) but otherwise contains no adjustable parameters.

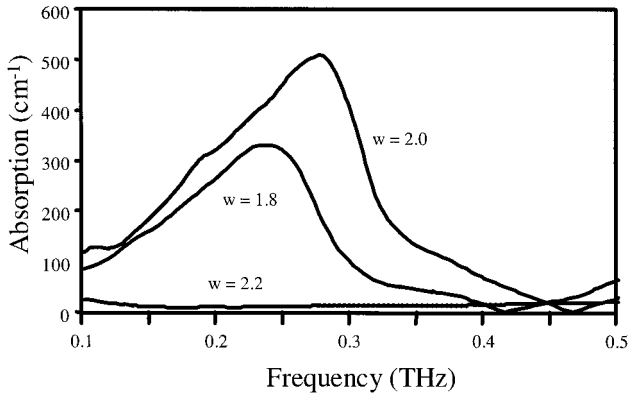

Figure 6. Absorption spectra of the polar core of three AOT micelle samples formed with glycerol rather than water in the interior, as described in the text. These have been derived from the raw data using the same formalism developed for H_2O micelles. Glycerol-containing micelles are stable over a much narrower range of w values, so an exhaustive size-dependent study is not possible. Nevertheless, the presence of absorption peaks in these samples is a clear indication of the generality of the phenomenon.

The role played by the Na^+ counterion in the formation of these absorption peaks merits investigation. For this reason, AOT samples containing brine were also characterized. A stock NaCl solution was made in Millipore water at 1.0 molar concentration of the Na^+ ion in water. Inverse micellar samples were then formulated according to the usual procedures. After the hydrated water micelles were formulated, the appropriate amount of 1 M saline was added to produce an inverse micelle with the desired w value and Na^+ concentration. Samples were made at w values of 10, 12, 15, and 17 with additional Na^+ concentrations ranging from 0.1 to 1 M. The larger micelles

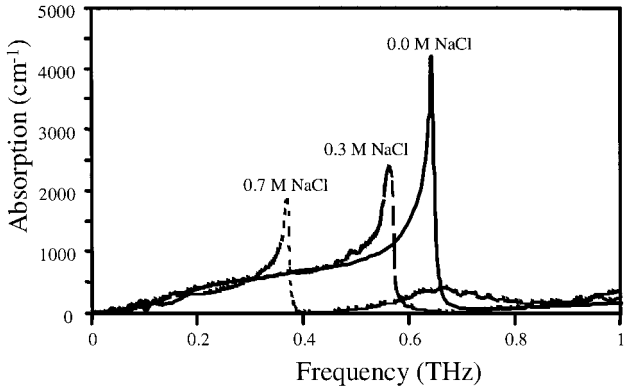

Figure 7. Absorption spectra of the aqueous core of three $w = 12$ micelle samples, formed with added salt in the aqueous core, at the specified concentration levels. The peak shift may be due to the variation of the micelle size with ion concentration.

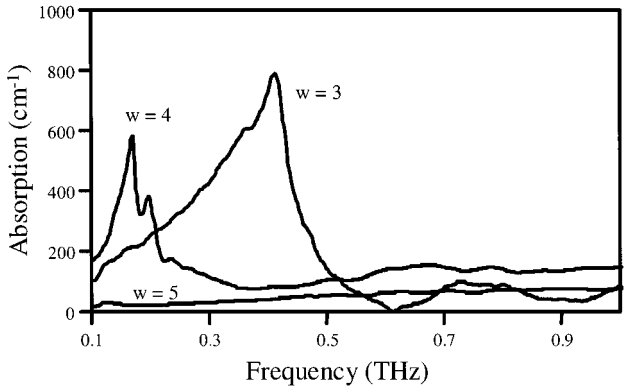

Figure 8. Absorption spectra of the polar core of several micelle samples formed using Brij-30, a nonionic surfactant. The observation of absorption peaks in these samples indicates that the resonance is likely not related to the presence of counterions in the core of the micelle.

were less able to solubilize the brine and tended to destabilize, immediately forming permanently cloudy phases. This tendency became more pronounced with higher salt concentrations. The 0.1 M concentration was soluble in all micelles tested. Only optically clear samples were analyzed using THz spectroscopy. Figure 7 shows absorption spectra for a typical sample, with varying salt concentration at $w = 12$. All of the brine samples exhibit the distinguishing resonant absorption present in the pure-water samples. As seen in Figure 7, the spectral location and amplitude of the resonance both shift with brine concentration, in a systematic fashion. This shift appears to arise from the variation in micelle size with increasing salinity. Further studies are underway to verify this hypothesis.

Inverse micelles with other surfactants have also been studied. This is an alternate method to address the role played by the counterion in the far-infrared spectra. Samples were formulated with Brij-30, a nonionic surfactant, in the concentration range from $w = 3$ to 6. Samples larger than $w = 6$ were cloudy or, in some cases, solidified, consistent with the phase diagram of the Brij/water/dodecane system.[58,19,59] As seen in Figure 8, these micelles formed with a nonionic surfactant also exhibit absorption peaks in the far-infrared. These peaks occur at frequencies lower than in the AOT samples of equivalent size. As in the AOT system, the largest Brij-30 samples do not show an absorption peak in their THz spectrum.

Despite the previously mentioned difficulty in forming nonhydrated reference samples using the CTAB/water/hexane-pentanol system, the far-infrared dielectric properties of this system were also investigated. Because quantitative results are difficult to obtain in this surfactant system, only a few samples were investigated. Nevertheless, it is notable that there were indeed absorption features in the spectra similar to those observed in other micellar systems.

Discussion

The experimental data shows unambiguously the presence of strong resonant far-infrared absorption in inverse micelles formed from a wide variety of solvents and surfactants. This resonance is remarkable for a liquid; water and other polar solvents in the bulk phase generally exhibit broad and featureless continuum absorption in this region. Thus, the feature must arise from some characteristic of the micelle. As we will discuss, it is confinement itself, not the surfactant or counterion, that gives rise to this absorption peak.

A striking feature of the observed peak is that it is found in nearly all micellar systems, regardless of the counterion or surfactant. This suggests it is an intrinsic property of confinement, rather than arising from a specific chemical functionality. Water pools containing Br^- counterions, Na^+ counterions, excess ions, and even water pools formed using nonionic surfactants all exhibit this strong far-infrared resonance, though the exact positions and shapes vary depending on the details of the micellar chemistry. Additionally, the existence of similar absorption features in nonaqueous liquid pools suggests that the origins of these peaks must not be exclusive to water alone.

As noted above, the integrated absorption strength in larger micelles is actually smaller than that of the bulk liquid in the spectral range from 0.1 to 1.3 THz. This suggests that the collective modes, which would be present at these frequencies in the bulk liquid, are absent in the confined liquid. This result is in marked contrast to the conventional description of the interior of large AOT micelles, which are generally described in terms of a "free" water pool with properties indistinguishable from that of the bulk.[21,27,60] This decreased integrated absorption suggests a dramatic redistribution of the density of modes of the system, relative to that of liquid water. This restructuring could also be related to the presence of the observed resonances. For this reason, we are motivated to consider the vibrational modes of a spherical liquid droplet.

The literature treatment of the vibrational modes of spherical objects is a rich and historic one. The first complete mathematical discussion of the dynamics of spherical liquid droplets was given by Sir Horace Lamb in 1879.[61] This model later proved an excellent basis for further development by a number of authors.[30,62−73] Many of these researchers have extended this theoretical treatment to specifically consider oil-in-water and water-in-oil microemulsions. For example, the polarizability of inverse micelles has been studied using depolarized light scattering and Kerr effect measurements.[74,75] These low-frequency results have been explained by invoking the presence of volume-preserving shape oscillations.[76,77] Yet, the high-frequency behavior, near the resonant frequency of these vibrational modes, has not been studied previously.

To predict the vibrational density of modes of a small liquid droplet, we adapt a model described by Tamura et al.[65] The discrete spherical modes can be separated into two distinct groups. Internal or compressional modes of the droplet consist of nonvolume-conserving fluctuations of the core of the droplet.[65] These modes correspond to confined acoustic vibrations of the liquid; their characteristic frequencies are therefore given by $\pi V/R_0$, where V is the sound velocity and R_0 is the droplet radius. Using the bulk value of the sound velocity of

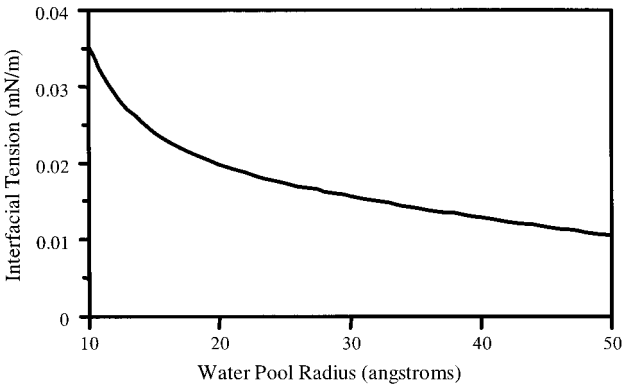

Figure 9. Interfacial tension at the $H_2O-AOT-$heptane interface, computed using the formalism developed by Peck and co-workers.[78] This reference provides not only the analytic expression for $\sigma(R)$ but also the values for all of the necessary parameters that enter into the computation of this quantity.

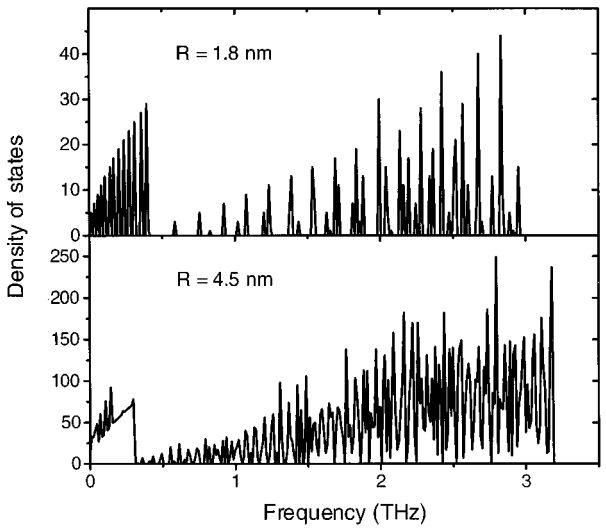

Figure 10. Density of states computed for two representative micelle sizes, using the formalism described in the text. These correspond to micelles with $w = 12$ (upper) and 30 (lower). The surface-localized modes, lying at low frequencies, are clearly separated from the internal compressional vibrations at higher frequencies. The high-frequency cutoff of the spectrum arises from the modified Debye criterion described in the text.

water, one finds that these modes fall at frequencies above 1 THz, too high to explain the enhanced far-infrared absorption observed experimentally. The other contributions to the spherical vibrational modes are those involving volume-conserving shape fluctuations of the droplet. The restoring force for these shape oscillations is not the bulk modulus, as in the acoustic modes mentioned above. Instead, the interfacial tension of the water−surfactant-oil interface acts as the restoring force; as a result, these modes have no analogue in the bulk liquid.[63,65,69,73] The surface oscillations are damped by the viscosity of the fluids on either side of the interface.[66] These shape changes take the form of surface corrugations, with angular frequencies given by

$$\omega_L = \sqrt{\frac{\sigma(R)\, L(L-1)(L+2)}{\frac{\rho_0 + \rho_1 L}{L+1} R^3}} \qquad (5)$$

Here, ρ_0 is the density of the water core, assumed to be the same as the bulk value (1 g/cm^3), and ρ_1 is the density of the surrounding fluid (in our case heptane, $\rho_1 = 0.684$ g/cm^3).[63] R is the radius of the water pool at the center of the micelle, and $\sigma(R)$ is the size-dependent interfacial tension between the two phases, mediated by the surfactant monolayer.

For the case of AOT, this interfacial tension has been discussed thoroughly by Peck and co-workers.[78] They derived a model calculation for $\sigma(R)$ that is comprised of contributions from the interactions between the surfactant tails and the organic solvent and the electrostatic contributions from the ionic headgroup-water interface. Figure 9 shows the size-dependent interfacial tension predicted by this model for our experimental system. This computation requires knowledge of several physical parameters of the AOT−water−heptane system such as the length of the AOT chain and its solubility in heptane, all of which can be found in the literature.[78] It is worth noting that this formalism predicts that the interfacial tension becomes negative at a size which corresponds approximately to the upper stability limit of the micelles. This lends additional credence to the validity of the model.

Given the resulting values for the interfacial tension of the water pool surface, it is possible to calculate the vibrational mode density of the spherical water droplet using eq 5. The total number of modes is computed using an argument similar to that of the Debye density of states, with an additional constraint on the maximum allowed value of the mode index L. This maximum value is determined by assuming that the wavelength of a vibrational mode must be no smaller than the mean intermolecular separation.[65] Figure 10 shows the calculated vibrational density of modes for two typical water pool radii, corresponding to $w = 12$ (upper panel) and 30 (lower panel). These calculations show the clear separation between the shape oscillations at lower frequencies and the confined bulk acoustic modes of the micelle at higher frequencies. We note that for the smallest micelles there is expected to be a coupling between the two types of vibrational modes, which modifies the computation somewhat.[65] We have verified that, for the parameters relevant in our experiments, this coupling results in only a very small modification of the computed density of modes and is therefore neglected.

Using these calculations, it is possible to predict the frequencies of the observed peaks by computing the mean frequency of the lower portion of the density of states (the part corresponding to the shape oscillations). This mean frequency, computed with no adjustable parameters, is plotted in Figure 4 (solid curve). For larger micelles, the agreement is surprisingly good considering the approximations inherent in this a priori model. It is also possible to compute the absorption strength, again using only the portion of the density of modes corresponding to the shape oscillations. A comparison with the amplitude of the experimental absorption peaks is complicated by a lack of knowledge of the oscillator strengths of the vibrational modes in the model. However, it is still instructive to compare the size-dependent trend. We compute the relative absorption strength by counting the fraction of the vibrational modes which correspond to shape oscillations, as a function of the water pool radius. This result is then scaled such that it matches the experimental data point of the sample with the largest radius. The predicted scaling with micelle size is shown in Figure 5 (solid curve). The calculation does predict an increase of the absorption strength at small radii, but as in Figure 4, it does not adequately predict the magnitude of this effect for the smallest micelle sizes.

It is notable that in both Figures 4 and 5 the agreement between the experimental data and the computation is much

better at larger radii. At smaller radii, the model apparently underestimates the predicted peak frequencies by more than a factor of 3. Given the lack of adjustable parameters in this model, such agreement is actually quite good. Still, it is instructive to consider why the model underestimates the peak frequencies.

Although several factors may be important, such as the breakdown of a vibrational continuum model in smaller sizes, it is more likely that fundamental parameters of importance to our model have different values from their bulk values in very small micelles. The calculated interfacial tension relies on parameters, such as the water density and static dielectric constant, for which we have used bulk values. Because it is known that the fraction of bound water is much larger in these small micelles, it is likely that these values are perturbed by the increasingly strained hydrogen-bond network of the confined water. It has been shown in high precision ultrasound velocimetry experiments by Amararene et al. that the compressibility of micellar bound water is reduced by a factor of 2 compared to that of free water.[79] These experiments also yielded a *w*-dependent volume for a single water molecule inside the micelle. This value was low at small *w* ($\sim$24 Å^3 at $w = 10$) and increased to the bulk value of $\sim$30 Å^3 by $w = 30$. Fluorescent probe experiments reported by a number of groups show that this bound water is highly immobilized and has an increased viscosity.[3,80,81] Finally, the spectral location of the librational band of bound water is shifted by approximately 25% with respect to the bulk value of 670 cm^{-1}.[33] All of these results point to the fact that the bound water, the predominate fraction in the smallest micelles, has a substantially different structure. It is not surprising that it would respond differently to compressional forces. This decrease in compressibility of bound water could lead to an enhanced coupling between the internal and surface-localized modes, which could in turn result in an increase in the mean vibrational mode frequency, as seen in Figure 4.

Another possible explanation for the deviation of the surface model from the data at small micelle sizes is coupling to the Debye relaxational modes of water. The second dielectric relaxation of bulk water, involving the motions of small numbers of water molecules, is located at $\sim$0.9 THz.[34] As the frequency of the surface oscillations approaches the frequency of this relaxational process within the aqueous core, it is plausible that these modes would exhibit some coupling. This could result in an increase in the amplitude of the absorption and could also tend to increase the peak frequency of the surface modes.

Incorporating liquids other than water into the core of the AOT inverse micelles provides a test of whether this effect would be expected to be observed in all liquids, or is a phenomenon unique to water. D_2O has a different molar mass than H_2O, and processes such as the O−H/O−D stretching frequencies in the infrared are strongly affected by this difference.[82] On the other hand, the far-infrared spectra of these liquids, where the dielectric function is dominated by correlated motions of groups of molecules, are quite similar.[83] The fact that the results for the D_2O/AOT system are nearly indistinguishable from those of the H_2O/AOT micelles (see Figure 4) is consistent with our model, which predicts no explicit dependence on the molecular mass of the internal species.

Despite having a limited stability range in which to formulate samples, the glycerol samples provide a crucial confirmation of the generality of the phenomenon. The fact that the peak is apparent in a significantly less polar liquid indicates that it is a property of a droplet and not a special attribute of water. Quantitative comparisons between a model and the experiment are not possible, because of a lack of complete characterization of this micellar system. However, the shift to lower frequencies of the peak in the glycerol sample is consistent with our expectations for a denser liquid with lower surface tension than bulk water. The surface tension of bulk glycerol is 0.63 mN/m as compared with 0.73 mN/m in bulk water.[84] The density of glycerol (1.261) is also a contributing factor to the shift of the glycerol peak to lower frequencies (see eq 5). If we assume that the surface oscillation model is equally valid for water and glycerol micelles, then we can regard the experimentally determined glycerol peak positions as a measurement of the surface tension of the glycerol−AOT−heptane interface. This analysis gives an interfacial tension of 8.0 mN/m for the 17.6 angstrom glycerol pool as compared to an interfacial tension of 21.2 mN/m in water pools of equivalent size. This value is reasonable given the lower polarity of the glycerol molecule and the lower value of the bulk surface tension in glycerol.

Conclusions

In conclusion, we report the observation of strong modifications to the frequency-dependent dielectric function of water confined in nanometer-sized pools. A pronounced terahertz resonance, such as the one reported here, has no precedent in bulk water or even most bulk liquids at normal temperatures. Its presence in inverse micelles and its strong size dependence suggest that it arises from the restricted dimensions of the micelle cavity. The mechanism proposed for these peaks involve surface oscillations of the confined liquid droplet. This model is able to predict the trends in the size dependence of the amplitude and spectral position of the experimental peak without adjustable parameters. The observation of this peak in micellar systems formed with H_2O, D_2O, brine, and glycerol provides further evidence for the generality of the phenomenon.

These findings have important implications for a host of chemical and biological processes in which sequestered water plays a role. In particular, the reaction dynamics of many different biochemical and catalytic processes occurring in confined geometries could be influenced by the vibrational modes of the confining vessel. Because solvent modes can play a crucial role in determining the rates of chemical reactions,[5,85] these results raise the intriguing possibility that the design of certain active molecular subunits may be optimized to exploit the enhanced vibrational density of states induced by the nanometer-scale confinement.

Acknowledgment. Mr. Jared Turner of Dianal America is gratefully acknowledged for performing the Karl Fischer analysis. This work has been funded by the National Science Foundation, the Robert A. Welsh Foundation, and the Petroleum Research Fund of the American Chemical Society.

References and Notes

(1) Atik, S. A.; Thomas, J. K. *J. Am. Chem. Soc.* **1981**, *103*, 4367−4371.

(2) Hilhorst, R.; Spruijt, R.; Laane, C.; Veeger, C. *Eur. J. Biochem.* **1984**, *144*, 459−466.

(3) Politi, M. J.; Chaimovich, H. *J. Phys. Chem.* **1986**, *90*, 282−287.

(4) Samama, J.-P.; Lee, K. M.; Biellmann, J.-F. *Eur. J. Biochem.* **1987**, *163*, 609−617.

(5) Vos, M. H.; Rappaport, F.; Lambry, J.-C.; Breton, J.; Martin, J. L. *Nature* **1993**, *363*, 320−325.

(6) García-Río, L.; Leis, J. R.; Iglesias, E. *J. Phys. Chem.* **1995**, *99*, 12318−12326.

(7) Swallen, S. F.; Weidemaier, K.; Fayer, M. D. *J. Phys. Chem.* **1995**, *99*, 1856−1866.

(8) Weidemaier, K.; Fayer, M. D. *J. Phys. Chem.* **1996**, *100*, 3767−3774.
(9) Consta, S.; Kapral, R. *J. Chem. Phys.* **1999**, *111*, 10183−10191.
(10) Bellissent-Funel, M.-C. *J. Mol. Liq.* **2000**, *84*, 39−52.
(11) Ahmed, S. I.; Friberg, S. *J. Am. Chem. Soc.* **1972**, *94*, 5196−5199.
(12) Corbin, D. R.; Herron, N. *J. Mol. Catal.* **1994**, *86*, 343−369.
(13) Johnson, J. W.; Brody, J. F.; Soled, S. L.; Gates, W. E.; Robbins, J. L.; Marucchi-Soos, E. *J. Mol. Catal. A* **1996**, *107*, 67−73.
(14) Pileni, M. P. *J. Phys. Chem.* **1993**, *97*, 6961−6973.
(15) Haram, S. K.; Mahadeshwar, A. R.; Dixit, S. G. *J. Phys. Chem.* **1996**, *100*, 5868−5873.
(16) Natarajan, U.; Handique, K.; Mehra, A.; Bellare, J. R.; Khilar, K. C. *Langmuir* **1996**, *12*, 2670−2678.
(17) Qi, L.; Ma, J.; Cheng, H.; Zhao, Z. *Coll. Surf. A* **1996**, *108*, 117−126.
(18) Zulauf, M.; Eicke, H.-F. *J. Phys. Chem.* **1979**, *83*, 480−486.
(19) Aveyard, R.; Binks, B. P.; Fletcher, P. D. I.; Ye, X. *J. Chem. Technol. Biotechnol.* **1992**, *54*, 231−236.
(20) Wong, M.; Thomas, J. K.; Nowak, T. *J. Am. Chem. Soc.* **1977**, *99*, 4370−4376.
(21) Maitra, A. *J. Phys. Chem.* **1984**, *88*, 5122−5125.
(22) Robinson, B. H.; Toprakcioglu, C.; Dore, J. C. *J. Chem. Soc., Faraday Trans. 1* **1984**, *80*, 13−27.
(23) Toprakcioglu, C.; Dore, J. C.; Robinson, B. H. *J. Chem. Soc., Faraday Trans. 1* **1984**, *80*, 413−422.
(24) Kotlarchyk, M.; Huang, J. S.; Chen, S.-H. *J. Phys. Chem.* **1985**, *89*, 4382−4386.
(25) Boicelli, C. A.; Giomini, M.; Giuliani, A. M. *Appl. Spectrosc.* **1984**, *38*, 537−539.
(26) MacDonald, H.; Bedwell, B.; Gulari, E. *Langmuir* **1986**, *2*, 704−708.
(27) D'Angelo, M.; Onori, G.; Santucci, A. *J. Phys. Chem.* **1994**, *98*, 3189−3193.
(28) D'Angelo, M.; Onori, G.; Santucci, A. *Il Nuovo Cimento* **1994**, *16*, 1601−1611.
(29) D'Angelo, M.; Martini, G.; Onori, G.; Ristori, S.; Santucci, A. *J. Phys. Chem.* **1995**, *99*, 1120−1123.
(30) Carlstrom, G.; Halle, B. *J. Phys. Chem.* **1989**, *93*, 3287−3299.
(31) Hauser, H.; Haering, G.; Pande, A.; Luisi, P. L. *J. Phys. Chem.* **1989**, *93*, 7869−7876.
(32) Ahlborn, H.; Ji, X.; Space, B.; Moore, P. *J. Chem. Phys.* **1999**, *111*, 10622−10632.
(33) Venables, D. S.; Huang, K.; Schmuttenmaer, C. A. *J. Phys. Chem. B* **2001**, *93*, 7409−7416.
(34) Kindt, J. T.; Schmuttenmaer, C. A. *J. Phys. Chem.* **1996**, *100*, 10373.
(35) Mel'nichenko, Y. B.; Schüller, J.; Richert, R.; Ewan, B.; Loong, C.-K. *J. Chem. Phys.* **1995**, *103*, 2016−2024.
(36) Bruni, F.; Ricci, M. A.; Soper, A. K. *J. Chem. Phys.* **1998**, *109*, 1478−1485.
(37) Crupi, V.; Magazu, S.; Majolino, D.; Migliardo, P.; Venuti, V.; Bellissent-Funel, M.-C. *J. Phys: Cond. Matter* **2000**, *12*, 3625−3630.
(38) Boyd, J.; Briskman, A.; Colvin, V.; Mittleman, D. *Phys. Rev. Lett.* **2001**, *87*, 147401.
(39) Martin, C. A.; Magid, L. J. *J. Phys. Chem.* **1981**, *85*, 3938−3944.
(40) Magid, L. J.; Martin, C. A. ^{13}C NMR studies of molecular conformations and interactions in the curved surfactant mololayers of aerosol OT water-in-oil microemulsions. In *Reverse Micelles: Biological and technological relevance of amphiphilic structures in apolar media*; Luisi, P. L., Straub, B. E., Eds.; Plenum Press: New York, 1982; pp 181−193.
(41) Fletcher, P. D. I.; Galal, M. F.; Robinson, B. H. *J. Chem. Soc., Faraday Trans. 1* **1984**, *80*, 3307−3314.
(42) Kotlarchyk, M.; Chen, S.-H.; Huang, J. S.; Kim, M. W. *Phys. Rev. A* **1984**, *29*, 2054−2069.
(43) Geiger, S.; Eicke, H.-F. *J. Colloid Interface Sci.* **1986**, *110*, 181−187.
(44) Giustini, M.; Palazzo, G.; Colafemmina, G.; Monica, M. D.; Giomini, M.; Ceglie, A. *J. Phys. Chem.* **1996**, *100*, 3190−3198.
(45) Mittleman, D. M.; Nuss, M. C.; Colvin, V. L. *Chem. Phys. Lett.* **1997**, *275*, 332−338.
(46) Rønne, C.; Thrane, L.; Åstrand, P.-O.; Wallqvist, A.; Mikkelsen, K. V.; Keiding, S. R. *J. Chem. Phys.* **1997**, *107*, 5319−5331.
(47) Smith, P. R.; Auston, D. H.; Nuss, M. C. *IEEE J. Quantum Elec.* **1988**, *24*, 255.
(48) van Exter, M.; Grischkowsky, D. *IEEE Trans. Microwave Theory & Technol.* **1990**, *38*, 1684.
(49) Garg, S. K.; Bertie, J. E.; Kilp, H.; Smyth, C. P. *J. Chem. Phys.* **1968**, *49*, 2551−2562.
(50) Pedersen, J. E.; Keiding, S. R. *IEEE J. Quantum Elec.* **1992**, *28*, 2518.
(51) Hanai, T.; Imakita, T.; Koizumi, N. *Colloid Polym. Sci.* **1982**, *260*, 1029−1034.
(52) Zhang, H. Z.; Sekine, K.; Hanai, T.; Koizumi, N. *Colloid Polym. Sci.* **1983**, *261*, 381−389.
(53) Zhang, H. Z.; Sekine, K.; Hanai, T.; Koizumi, N. *Colloid Polym. Sci.* **1984**, *262*, 513−520.
(54) Sekine, K. *Colloid Polym. Sci.* **1986**, *264*, 943−950.
(55) Sekine, K. *Colloid and Polym. Sci.* **1987**, *265*, 1054−1060.
(56) Jackson, J. D. *Classical Electrodynamics*, 2nd ed.; John Wiley & Sons: New York, 1975.
(57) Faeder, J.; Ladanyi, B. M. *J. Phys. Chem. B* **2000**, *104*, 1033−1046.
(58) Podo, F.; Ray, A.; Nemethy, G. *J. Am. Chem. Soc.* **1973**, *95*, 6164−6171.
(59) Merdas, A.; Gindre, M.; Ober, R.; Nicot, C.; Urbach, W.; Waks, M. *J. Phys. Chem.* **1996**, *100*, 15180−15186.
(60) Onori, G.; Santucci, A. *J. Phys. Chem.* **1993**, *97*, 5430−5434.
(61) Lamb, S. H. *Hydrodynamics*, 6th ed.; Cambridge University Press: Cambridge, U.K., 1932.
(62) Tamura, A.; Higeta, K.; Ichinokawa, T. *J. Phys. C: Solid State Phys.* **1982**, *15*, 4975−4991.
(63) Ljunggren, S.; Eriksson, J. C. *J. Chem. Soc., Faraday Trans. 2* **1983**, *80*, 489−497.
(64) Safran, S. A. *J. Chem. Phys.* **1983**, *78*, 2073−2076.
(65) Tamura, A.; Ichinokawa, T. *Surf. Sci.* **1984**, *136*, 437−448.
(66) Milner, S. T.; Safran, S. A. *Phys. Rev. A* **1987**, *36*, 4371−4379.
(67) Lebedev, V. V.; Muratov, A. R. *Sov. Phys. JETP* **1989**, *68*, 1011−1022.
(68) Sparling, L. C.; Sedlak, J. E. *Phys. Rev. A* **1989**, *39*, 1351−1364.
(69) Lisy, V. *Phys. Lett. A* **1990**, *150*, 105−112.
(70) Duval, E. *Phys. Rev. B* **1992**, *46*, 5795−5797.
(71) Earnshaw, J. C.; McLaughlin, A. C. *Proc. R. Soc. London A* **1993**, *440*, 519−536.
(72) Lisy, V. *Phys. Rev. E* **1994**, *50*, 3755−3765.
(73) Eriksson, J. C.; Ljunggren, S. *Langmuir* **1995**, *11*, 1145−1153.
(74) Borkovec, M.; Eicke, H.-F. *Chem. Phys. Lett.* **1989**, *157*, 457−461.
(75) van der Linden, E.; Geiger, S.; Bedeaux, D. *Physica A* **1989**, *156*, 130−143.
(76) Borkovec, M.; Eicke, H.-F. *Chem. Phys. Lett.* **1988**, *147*, 195−202.
(77) van der Linden, E.; Bedeaux, D.; Borkovec, M. *Physica A* **1989**, *162*, 99−110.
(78) Peck, D. G.; Schechter, R. S.; Johnston, K. P. *J. Phys. Chem.* **1991**, *95*, 9541−9549.
(79) Amararene, A.; Gindre, M.; Huérou, J.-Y. L.; Urbach, W.; Valdez, D.; Waks, M. *Phys. Rev. E* **2000**, *61*, 682−689.
(80) Hasegawa, M.; Sugimura, T.; Suzaki, Y.; Shindo, Y.; Kitahara, A. *J. Phys. Chem.* **1994**, *98*, 2120−2124.
(81) Pant, D.; Riter, R. E.; Levinger, N. E. *J. Chem. Phys.* **1998**, *109*, 9995−10003.
(82) Walrafen, G. E. Raman and Infrared Spectral Investigations of Water Structure. In *Water A Comprehensive Treatise*; Franks, F., Ed.; Plenum Press: New York, 1972; Vol. 1, pp 151−214.
(83) Rønne, C.; Astrand, P. O.; Keiding, S. R. *Phys. Rev. Lett.* **1999**, *82*, 2888−2891.
(84) Ebbing, D. D. *General Chemistry*, 4th ed.; Houghton Mifflin Company: Boston, 1993.
(85) Liebl, U.; Lipowski, G.; Négrerie, M.; Lambry, J.-C.; Martin, J.-L.; Vos, M. H. *Nature* **1999**, *401*, 181−184.